Journal of Building Engineering 51 (2022) 104186

Contents lists available at ScienceDirect

Journal of Building Engineering

journal homepage: www.elsevier.com/locate/jobe

Pozzolanic and hydraulic activity of bauxite for binder production

O. Alelweet, S. Pavia *

Dept. of Civil Engineering, University of Dublin, Trinity College Dublin, Ireland

ARTICLE INFO

Keywords:
Bauxite
Pozzolanic activity
Thermal activation
Kaolinite
Boehmite

ABSTRACT

Bauxite is mainly used to produce aluminium and calcium aluminate cements. Both applications carry high environmental impacts. However, the carbon emissions generated from mining bauxite (3–5 kg CO_2e/t) are negligible when compared those generated for aluminium or cement production (620–700 kg CO_2e/t for CEM II). Hence, an alternative use for bauxite would lower environmental impacts worldwide. This paper measures the pozzolanic and hydraulic capacity of raw and thermally activated bauxite with a view to use it, as a binder, in construction.

The results indicate that the bauxite is pozzolanic and, when fired over 900 °C it becomes slightly hydraulic. An amorphous reactive phase begins to appear at 300 °C, but the lime binding potential is enhanced at 550 °C because most of the aluminium is in amorphous form. Some active phases (except for ϒ- Al_2O_3) could not be detected with XRD due to their amorphousness. However, their pozzolanicity was evidenced with direct and indirect measurements.

The bauxite's pozzolanic and mechanical indices are high, comparable or superior to other pozzolanic and cementing materials. Gibbsite, boehmite and kaolinite are the main phases in the bauxite. Their layered atomic structures with high specific surface areas (SSA) and active surface hydroxyls that enhance adsorption, and hence nucleation, precipitation and dissolution, provide a high pozzolanic activity. The high kaolinite content, and the presence of the highly-reactive, kaolinite-polymorph nacrite, enhance reactivity, and the presence of sulphates also contributes to the initial activity.

The SSA of the bauxite particles, is superior to CEM II and other pozzolanic and cementing materials, and heating, even at low temperature (300 °C), drastically increases the SSA of the particles (by~60%). The methods that determine initial pozzolanic activity rate the 550 °C bauxite as the most active, while the mechanical methods rate the 700–800 °C bauxites as the most reactive. This is because the high SSA of the 550 °C bauxite enhances lime combination in the earlier stages of the pozzolanic reaction, while the 700–800 °C bauxite has the highest amorphous/active alumina content which control late pozzolanic activity. As evidenced with XRD, at 700–800 °C, boehmite has disappeared, transformed into amorphous transition aluminas, and kaolinite has completely turned into reactive metakaolin.

1. Introduction

One of the most important objectives that need to be reached worldwide to protect the environment, is to reduce emissions of greenhouse gases such as carbon dioxide, nitrous oxide and methane which are responsible for the greenhouse effect. The principal binder used in construction for decades has been cement, mainly Portland cement- PC. The high environmental impact of PC is due to

* Corresponding author.
E-mail addresses: alelweeo@tcd.ie (O. Alelweet), pavias@tcd.ie (S. Pavia).

https://doi.org/10.1016/j.jobe.2022.104186
Received 15 December 2021; Received in revised form 28 January 2022; Accepted 5 February 2022
Available online 10 February 2022

its high embodied energy and high embodied carbon dioxide emissions resulting from clinker production. The extensive use of PC in construction over the last centuries, is one of the main responsible for the high global CO_2 emissions of the construction industry. In this context, the search for alternative construction binders that can replace cements of high environmental impact is an important research subject

This paper investigates the potential of bauxite as a binder. The bauxite investigated is sourced from the Az Zabirah and Al Bai'tha mines in the Al Qassim and Hail provinces of Saudi Arabia. The pozzolanic and hydraulic activity of raw and thermally activated bauxite is measured with direct and indirect methods. The paper also compares the environmental impact of bauxite mining with that of cement production. The impact considers the energy required for mining bauxite (both in general and specific to the Saudi bauxite) and compares it with that required for producing PCs including CEM I and CEM II. The greenhouse gas -GHG-emissions generated are expressed as global warming potential- GWP- in kg CO_2e/t.

Bauxite has been fused together with lime and limestone, and grounded, to produce high-alumina cements, also known as aluminous cements and calcium aluminate cements (CACs), which consist mainly of calcium aluminates. Most CAC manufacturing processes reach kiln temperatures of 1450 °C and above [1], hence they have embodied energy and GHG emissions even greater than those of PC clinker. Furthermore, CACs are very hard to grind, leading to high power consumption and heavy wear of the grinding equipment which increase their environmental impact.

This paper does not fuse the bauxite with any calcium sources, but it attempts to sinter the bauxite alone at increasing temperature (200–1000 °C) and determine the resultant pozzolanic and/or hydraulic activity. The temperatures are kept relatively low to reduce environmental impact.

The majority of mined bauxites are lateritic, and mainly consist of hydrates of alumina. Their main mineral component is usually gibbsite $Al(OH)_3$, with smaller amounts of boehmite, γ-AlO(OH), and often diaspore α-AlO(OH). Clays such as kaolinite $Al_2Si_2O_5(OH)_4$ as well as iron oxides (hematite Fe_2O_3, goethite FeOOH), silica (quartz SiO_2), and titania (rutile TiO_2 or anatase TiO_2) are usually present in lesser amounts.

In the Az Zabirah bauxite subject to study, gibbsite, boehmite and kaolinite are predominant minerals, and the bauxite has low iron and low organic matter contents [2,3].

The layered atomic structures of gibbsite and boehmite are comparable to the structures of clays such as kaolinite: their high specific surfaces and active hydroxyl surfaces makes them highly reactive, and hence suitable for a wide range of applications such as adsorbents and catalysis supports.

Their high specific surfaces enhance adsorption (accumulation of matter at the solid/water interface) which affects the rates of nucleation, precipitation and dissolution, and the catalysis of redox processes [4], therefore increasing reactivity.

The surface hydroxyl groups (adsorbed water molecules in dissociated form) of gibbsite and boehmite are active centres in many reactions [5]. Their amount and nature affect the physicochemical properties of the surface and the efficiency as a catalyst or adsorbent [6]. The bonds between adjacent hydroxyl ions can weaken, increasing layer separation and causing their breakup, producing an enhanced reactivity. This has been evidenced in boehmite -n-AlO(OH)- by Brühne et al. [7].

As well as being Al ores, gibbsite and boehmite are precursors for the production of transition aluminas such as γ-/δ-Al_2O_3, χ-Al_2O_3 and corundum (α-Al_2O_3) which are used in industries including filler, catalysis, glass, ceramics, purification, paint, coating, medicine and metallurgy and light-emitting diodes (LEDs) [8]. Gibbsite is the most important precursor of alumina powders for advanced and traditional ceramics, catalysts and adsorbents [9].

As it can be seen from the above, the alumina hydrates (or aluminum oxyhydroxides) in bauxites are reactive. They have multiple industrial applications, and their transitions have been studied by former authors. Most studies refer to the phases in synthetic form, as laboratory-synthesized, structurally and chemically precise, pure, nanoplates of gibbsite and boehmite with no detectable structural defects. However, in naturally occurring bauxites, the alumina hydrates are mixed with other phases such as gypsum and iron oxides, and soluble phases such as gypsum affect reactivity. Furthermore, former authors have studied the atomic structures of gibbsite and boehmite and their transformation in detail, but they don't establish a direct correspondence between the microstructural changes and the variation in the physicochemical properties of the surface that determine adsorption and reactivity, and hence control their application as a binder in construction. This paper intends to establish the pozzolanic and hydraulic cementing abilities of the aluminium oxyhydroxides naturally occurring in the Saudi Arabian bauxite and establish their potential as a binder in construction.

2. A comparative study of the environmental impact of bauxite mining and cement production

Bauxite is the principal ore for aluminium. Extraction is adjusted to local conditions and is carried out mechanically or with explosives. The environmental impact of producing aluminium from bauxite is high, and the GHG emissions arising from the process are an environmental concern. However, the bauxite mining emissions are negligible when compared to the rest of emissions generated during aluminium production. Georgitzikis et al., [10] indicate that, of the total GHG emissions (16.6 tonnes of CO_2e per tonne of primary Al), electrolytic smelting is responsible for 12.8 tonnes while mining only accounts for 0.05 tonnes of CO_2e per tonne of Al. The majority of the emissions of aluminium production (61%) arise from the electricity that powers electrolysis during the smelting process, while the rest (39%) arise for all the other steps in production including mining, refining (or Al_2O_3 production) and semis production (i.e. sheet, strip, plate, profiles, rod and bar, tube, wire and forgings) (Georgitzikis et al., based on data by the International Aluminium Institute -IAI- dating from 2020). On view of these results, and despite the wide use and numerous applications of aluminium in today's world, it can be argued that an alternative use for bauxite (other than Al production) would lower environmental impacts worldwide. This paper investigates the potential of bauxite as a binder by measuring the pozzolanic and hydraulic activity of raw and thermally activated bauxite.

Norgate and Haque [11] carried out a comparative study of the environmental impact of mining operations, indicating that bauxite mining uses considerably less energy and has much lower impact than iron ore or copper concentrate mining. The impact categories considered gross energy requirement (or embodied energy) and GHG emissions expressed as global warming potential- GWP). The authors included: drilling equipment (explosive loader trucks and several types of drills run with electricity and diesel power); the energy consumed in the blasting process derived from the chemical energy contained in the blasting agents; excavators; pumping for dewatering; dump trucks; and auxiliary equipment such as dozers, graders, excavators and water tankers used for road construction, maintenance and dust suppression. The authors also considered crushing and grinding plants (usually powered by electricity generated onsite using diesel generator) and assorted physical separators when needed or just screening (for bauxite). They note than most of these assets use diesel fuel for their operation. The results evidenced that bauxite mining requires much lower energy (54.9 MJ/tonne)

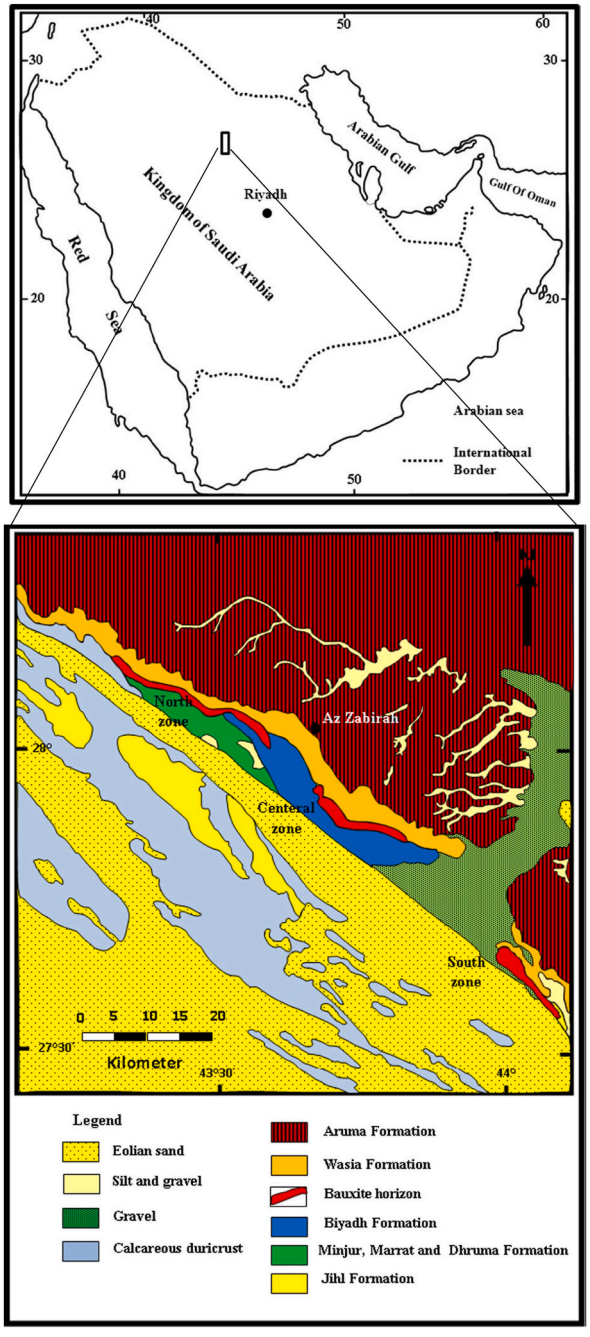

Fig. 1. Location of the Az Zabirah area and geological map of the Az Zabirah bauxite deposits by Al-Mutari, Galmed and Aldamegh [3]. Reproduced with the authors' permission.

than mining copper and iron ore (at 8329.0 and 152.7 MJ/tonne of ore respectively). Therefore, the embodied energy of mining bauxite is much lower than that of mining other ores. Furthermore, the authors state that the GWP of bauxite mining (4.9 kg CO_2e/t) is also much smaller than those of mining copper and iron ore (628.0 and 11.9 kg CO_2e/t ore respectively) [11].

This paper is based on the quarrying of the Az Zabirah and Al Bai'tha mines. The Az Zabirah mine supplies kaolin to the phosphate industry and low-grade bauxite to local cement companies, while the Al Bai'tha is quarried for high-grade bauxite for aluminium production [12]. Details of the mining process, as provided by (B.A.M. Sidiya, Kaolin Processing and Management Ma'aden, 2021) [13], are included in the Materials section below. As it can be seen from these details, the primary energy used in bauxite quarrying is diesel. The CO_2 emissions, estimated based on the quantity of diesel used and the activity of the Alzabirah mine, amount 3.3 kg CO_2/t bauxite. This calculation considers a diesel consumption of 3144 l/day producing 8237.3 kg CO_2 [13].

The construction binder that generates the highest CO_2 emissions is Portland cement (PC) clinker. The CO_2 emissions from PC clinker production are a function of the energy efficiency of the calcination process and the type and consumption of fuel, with literature reporting a variation between 821.1 and 1150 kg CO_2/t clinker [14]. A world average emission of 1 ton CO_2/t clinker is generally adopted, which in some cases is an overestimation because many producers currently have technologies to mitigate emissions, hence achieving emissions below 800 kg CO_2/t clinker [14].

CEM I is the PC which contains the most clinker (95%), hence it carries the greatest environmental impact. The reported GWP of CEM I, measured for an average tonne of cement CEM I 52.5 (produced by 12 different companies across the 9 countries), is 874 kg CO_2e [15]. However, CEM I is hardly used in many countries in Europe because it is often over-specified for many applications, and it has a high environmental impact. Much more used is CEM II, which incorporates limestone as partial clinker substitution lowering environmental impact. However, the average tonne of CEM II still releases significant CO_2 into the atmosphere (620–700 kg CO_2e - [15]). This is a lower emission than CEM I, however still enormous when compared to the 3.3 kg CO_2e/t bauxite calculated for the Alzabirah mine and the 4.9 kg CO_2e/t bauxite reported by Norgate and Haque [11] for general bauxite mining. Furthermore, the (CO_2) greenhouse gas (GHG) emissions of the cement industry contributing to global warming is not the only environmental impact of cement production but, as pointed out by García-Gusano et al. [16], photochemical ozone formation, acidification and fresh-water eutrophication can also be linked to the cement industry.

3. Materials and methods

The bauxite was quarried from a deposit located in a remote desert area of central/northern Saudi Arabia, predominantly in the province of Ha'il (Fig. 1). The Ma'aden's exploration area covers approximately 6000 km^2, centered in the town of Az Zabirah (northwest of Riyadh), with elevations of 535–600 m above sea level [2,3] indicate that the bauxite layers have a similar mineralogy, and that their main textures are microoliths, ooliths and pisoliths which are composed largely of boehmite and often have gibbsitic rims. They also refer to calcite as a significant secondary mineral in the bauxite, found in cavities and cracks as a cementing material.

The bauxite was studied both raw and grounded in a digital ball mill with 20 mm Ø stainless steel balls at 150 r.p.m. The bauxite was first grounded for 24 h, and the fraction under 0.5 mm was further grounded for 3 h. The grounded bauxite was calcined at increasing temperatures and used for all the tests. The lime used is a hydrated lime of European designation CL90s.

The Az Zabirah and Al Bai'tha mines are open-pit operations located approximately 20 km apart, North of the city of Qibah, in the Al Qassim and Hail provinces of central Saudi Arabia (Fig. 1). Al Mutari et al., [3] carried out a comprehensive study of the area. According to the authors, the Az Zabirah bauxite is a Cretaceous paleolaterite, and the Mesozoic sediments were deposited on a stable platform without any major tectonic disturbances. However, they were later uplifted, exposed and eroded due to Quaternary activity [3]. The bauxite deposits are discontinuous, uplift associated with the faulting has caused the erosional loss of the bauxite sequence [3] (Fig. 1). The bauxite is ovelaid by the Upper Cretaceous Wasia Formation and the Aruma Limestone, and the area has a NW-SE strike over a length of approximately 105 km, with succession of dips of approximately 5° towards the NE [3].

As aforementioned, the primary energy used in bauxite quarrying and production is diesel fuel [13]. The mining process starts with stripping the overburden by bulldozer ripping and dozing. The strip waste is then loaded into dump trucks and hauled to dumps outside the pit. Once exposed, the bauxite is ripped and piled in heaps by bulldozer. The ore is then screened and blended to meet customer requirements in terms of size and chemistry. Finally, the product is loaded into trucks and dispatched to costumers. During overburden stripping, a 0.5–1 m soil cap is removed with a bulldozer, loaded into trucks and send to landfill. Following overburden removal, the bulldozer rips the bauxite layer (0.5 m per pass) and gathers it in heaps. The mine utilizes Cat D9R bulldozers for both the overburden and the ore. The material is then hauled to blending areas for screening and blending. All the batches are sampled and analysed for chemical specification. The screening is carried out using front end wheel loaders and mobile screens. The loaders collect the material passing the sieve and stockpile it as the final product. Auxiliary equipment includes one grader and one compactor for road maintenance.

3.1. Composition and physical properties of the bauxite

The elemental chemical composition of the bauxite was analysed quantitatively with X-Ray fluorescence analysis using a ThermoFisher Scientific and Edwards analytical apparatus that used a Quant'X EDX spectrometer and an UniQuant analysis package. The results were uttered in oxide form as % by weight. The organic matter content was estimated by calculating the loss on ignition (LOI). The mineral composition of the raw and pyro-processed bauxite were studied with X-Ray diffraction (XRD), with a Phillips PW1720 XRD apparatus equipped with a PW1050/80 goniometer and a PW3313/20 Cu k-alpha anode tube, the running conditions were 40 kV and 20 mA. The measurements were taken between 5 and 60° (2θ) at a step size of 0.02°/second.

The particle size was measured by laser diffraction using a Malvern Mastersizer 2000 system. The specific surface area (SSA) was

determined with a Quantachrome 4200 e apparatus using the Brunauer Emmett Teller (BET) theory. The SSA of the sintered bauxites was also measured to assess the effect of the thermal treatment on the SSA.

The bauxite was studied with differential scanning calorimetry (DSC) and thermal gravimetric analysis (TGA). The TGA and the DSC of the bauxite were carried out using refractory alumininum crucibles, calcined at temperatures ranging from 200 to 1000 °C, in a fibre-chamber, 10 L furnace reaching up to 1300 °C. The DSC analyses indicate thermal events (crystallization, dehydroxilation, combustion), as exothermic or endothermic peaks while TGA shows the weight loss, or change in mass due to dehydration, decarbonation or oxidation, over a temperature range.

3.2. Phase conversion and specific surface area transformation on sintering

The bauxite was calcined in small batches, in an electric furnace at temperatures ranging from 200 to 1000 °C. The sintering time was 3 h. The crystalline phases produced as a result of the pyro-processing were determined with XRD analysis as explained above. The variation of the specific surface area with raising temperature was determined with a Quantachrome 4200 e apparatus using the Brunauer Emmett Teller (BET) theory as explained above for the raw bauxite.

3.3. Water demand and setting times

The setting times of bauxite: lime pastes were measured with the Vicat test (EN 196–3) [17] which determines the stiffening rate of a paste by dropping a needle from a fixed height and measuring its penetration. The variation in the stiffness of the bauxite: lime pastes and their eventual hardening are determined by hydrate formation (resulting from pozzolanic and/or hydration reactions), carbonation and mechanical processes such as flocculation and drying. The initial and final setting times are standard references which provide comparative data. The Vicat test was carried out on lime: bauxite pastes, in the ratios 1:1. The water demand of the raw and the sintered bauxites was determined by fixing the initial flow diameter at approximately 170±5 mm. The initial flow diameter was chosen because it provided a good workability and ensured a standard consistency.

3.4. Evaluation of reactivity with mechanical methods: strength and mechanical index

Reactivity indicates how quickly a material would combine lime (calcium hydroxide) in a pozzolanic reaction, or water in hydration reactions, to form cementing hydrates that would induce setting and eventually hardening. Compressive strength, and hence the mechanical activity index, is not only dependant on the amount of hydrates formed but also on their type and microstructure.

Mechanical test were carried out to compare the strength of standardised prismatic specimens of dimensions 160 × 40 × 40mm. The strength of standard mixes made with raw and sintered bauxites were measured and compared. The specimens were demoulded after three days and cured under damp hessian to maintain humidity, in a curing chamber at ambient temperature and 60 ± 5% relative humidity. The flexural strength was assessed following EN 196–1 [18]. The results are the arithmetic mean of six specimens for compressive strength and three for flexural strength.

The mechanical index (MI) was also calculated. It evaluates reactivity by measuring the compressive strength of the lime: bauxite mixes in relation to a standard lime mix after 28 days of curing. The MI is adapted from EN 450-1-Fly ash (FA) for concrete [19]. The prisms were produced with a ratio by mass of 1:1:3 (lime: bauxite: sand) with w/b = 0.90 ± 0.20. The 1:1 (lime: bauxite) content was chosen to be able to compare the results with former literature on pozzolan reactivity [20].

3.5. Evaluation of pozzolanic activity with chemical methods: conductivity variation

This method evaluates the pozzolanic reaction of the raw and pyro-processed bauxites indirectly by measuring the changes in the conductivity of a saturated lime/bauxite solution. It follows the method by De Luxan et al., and Paya et al., [21,22]. The fixation of dissolved $Ca(OH)_2$ reduces portlandite concentration in solution, leading to a decrease in conductivity. The conductivity variation of the lime-bauxite suspension was measured over time to examine the bauxites' ability to combine lime, and therefore their reactivity. Continuous stir took place using magnetic stirrer, conductivity and temperature were measured over time using WTW LF 197 conductivity meter with a Tetracon 325 probe. The solutions were kept in sealed flasks to avoid water evaporation and carbonation. The reaction was followed for over 170 h. The flasks containing the solutions were kept in a thermostatic bath to maintain a constant temperature of 20 °C. The temperature was maintained because very small variations in temperature (as low as 0.3 °C) induce considerable conductivity variation [21]. The conductivity loss over time was plotted, and the conductivity variation calculated as a percentage.

3.6. Direct measurement of pozzolanic activity with the chappelle test

The pozzolanic activity was also directly quantified by measuring the amount of calcium hydroxide (portlandite-$Ca(OH)_2$) fixed by the bauxites (pozzolanic index) in accordance with the methods in Gava and Prude and NBR 15895 [23,24]. The test results were compared with pozzolanic (FA) and cementitious materials (GGBS) previously studied by the authors. Solutions were fabricated with each bauxite, lime and distilled water, and a blank test containing only CaO was also included.

Sucrose was added and stirred, and the resultant solution titrated with 0.1 M HCl. The HCl volume consumed in titration (V2) was noted as well as that consumed by the blank test (V3). The pozzolanic activity index ($I_{Ca\ (OH)2}$) or amount of portlandite (mg) fixed per gram of bauxite, was calculated with equation (1):

$$I_{Ca(OH)2} = \frac{28\ (V_3 - V_2)\ Fc}{m_2} \tag{1}$$

Where: m_2 is the mass of bauxite (g).

V2 is HCl 0.1 M volume consumed by titration (ml), V3 is the HCl 0.1 M volume consumed in the blank test, Fc is a correction factor (Fc = 1.32 - for a HCl concentration of 0.1 M).

As aforementioned, the portlandite content that was not consumed was determined by sucrose extraction and HCl titration. The HCl can dissolve some calcite, gypsum and goethite which are components of the raw bauxite, therefore, the reactivity can be underestimated at the low calcination temperatures.

3.7. Microstructure and hydrate formation by scanning electron microscopy (SEM)

The microstructure of the bauxite/lime pastes and the nature and presence of hydrates was investigated with a SEM system. The elemental composition of the new formed hydrates was determined with EDXRA. The qualitative nature of the SEM study did not allow to establish quantitative trends on the nature of the phases formed upon hydration or the quality and distribution of the hydrates in the different pastes. However, representative microstructures and hydrates were recorded and are shown in the SEM results.

4. Results

4.1. Physical properties of the bauxite

The specific surface area (SSA) measured with BET, laser grading, particle density and loss on ignition are included in Table 1. The properties are compared with those of other pozzolanic and cementitious materials such as GGBS, FA and Portland cement (CEM II). As it can be seen from the results (Table 1), the bauxite consists of dense particles of extremely high SSA, and the organic matter content is insignificant. As aforementioned, the bauxite was studied both raw and grounded in a digital ball mill with 20 mm Ø stainless steel balls, and the grounded bauxite was calcined and tested.

In the case of the raw, unmilled bauxite, despite being coarser that typical pozzolanic and cementing materials (90% of the particles are smaller than 464 μm and only 10% are under 1.22 μm), the raw bauxite particles have a high specific surface area, superior to commercial PC (CEM II) and other pozzolanic and cementing materials such as FA (fly ash) and GGBS (ground granulated blast-furnace slag). The high SSA of the bauxite, even raw (unmilled), is due to the layered atomic structures of the bauxite's main components (gibbsite, kaolinite and boehmite). The grounded bauxite is much finer, as 90% of its particles are under 116 μm, 50% under 21.6 μm and 10% under 0.96 μm.

Heating significantly increases the SSA of the bauxite particles even at low temperature: at 300 °C the SSA has increased by over 60%. The specific surface area of the bauxite particles increases with increasing calcination temperature up to 700 °C and then lowers (Table 2). The bauxite displays the maximum SSA when calcined between 300 and 700 °C. However, the SSA is also high at 800 °C, showing a similar value. Therefore, the thermal treatment of the bauxite increases the surface available for reaction at least up to 700 °C. The results indicate that, at a certain point after reaching 700 °C, the bauxite particles begin to agglomerate. A similar trend was obtained when sintering the red mud residue of this bauxite [25]. Other authors have also found similar trends in other bauxites. Vieira Coelho et al. [26] observed the maximum specific surface area for a bauxite calcined between 300 and 400 °C.

4.2. Chemical and mineral composition of the bauxite

According to the XRF analyses (Table 3), aluminium is the most abundant element in the bauxite followed by silicon. Iron and titanium follow in much lower amounts. The rest of the elements are marginal except for the calcium and sulphur (2%). The variability in the XRF results reflects the extent of the outcrops and the timing of the analyses being wide apart.

The mineralogical composition of the bauxite is included in Fig. 2 and summarised in Table 4. The XRD trace indicates high crystallinity, presenting clear and intense reflections for the main phases which include gibbsite, kaolinite and boehmite. The relative intensities of their main reflections suggest that the amount of gibbsite is close to the amount of kaolinite, and that the amount of boehmite is at least 50% lower. According to the XRD results, kaolinite, boehmite and gibbsite are major phases (40-15%) while goethite, gypsum, rutile/anatase and calcite are minor components (15-7%) and there are traces of quartz (<7%).

The kaolinite polymorph nacrite [$Al_2Si_2O_5(OH)_4$] was identified. Similarly to kaolinite, it is a 1:1 clay mineral, hence its primary structural unit is a layer consisting of one octahedral sheet (with the octahedral site occupied by aluminium) condensed with one tetrahedral silicon sheet, and these layers are regularly stacked. Nacrite is the rarest of the four kaolinite polymorphs and occurs mostly in hydrothermal environments [27,28]. Nacrite dehydroxylates similarly to kaolinite, but their atomic structures slightly differ. Nacrite has a greater interlayer separation and smaller lateral dimension than kaolinite, and the position of the basal O atoms differ. As

Table 1
Specific surface area of the raw and grounded bauxite compared with other pozzolanic and cementitious materials. (*) grounded.

	Specific surface area (SSA) m^2/g	Particle density mg/m^3	Particle size distribution			LOI %	
			D90 μm	D50 μm	D10 μm	450 °C	1000 °C
Bauxite	17.92	2.43	463.94	74.10	1.22	0.30	1.10
Bauxite (*)	32.00	2.43	116.00	21.60	0.96	0.30	1.10
RM	9.35	2.94	8.42	3.80	0.40	5.04	11.51
GGBS	1.95	1.80	31.62	11.67	2.35	0.41	−0.77
FA	6.50	2.28	100.63	14.96	1.95	1.67	4.92
CEM II	1.88	–	82.58	24.90	2.56	–	–

Table 2
Effect of increasing temperature on the specific surface area of the grounded bauxites.

Material	SSA (m^2/g)
Bauxite 300 °C	81.81
Bauxite 550 °C	82.26
Bauxite 700 °C	82.53
Bauxite 800 °C	80.00
Bauxite 900 °C	67.00
Bauxite 1000 °C	40.38

Table 3
Chemical composition analysed by X-ray fluorescence (XRF) expressed as % wt. (*)- Arithmetic mean of the bauxite samples analysed 1 and the analyses provided by the producer 2. RM-Red Mud residue. ** Alelweet et al., 2021 [25].

	SiO_2	Al_2O_3	CaO	Fe_2O_3	Na_2O	K_2O	MgO	P_2O_5	SO_3	Cl^-	TiO_2	MnO
Bauxite[1]	26.82	54.30	2.48	6.01	0.008	0.23	0.00	0.59	2.89	0.25	5.62	0.01
Bauxite[2]	14.85	52.53	1.15	4.00	0.19	0.06	0.13	0.13	1.57	–	4.78	<0.01
Bauxite (*)	21.00	53.00	2.00	5.00	0.10	0.10	0.06	0.40	2.00	0.25	5.00	0.01
RM (**)	19.66	29.79	5.09	12.97	24.05	0.09	0.40	0.29	1.65	0.32	5.12	0.02

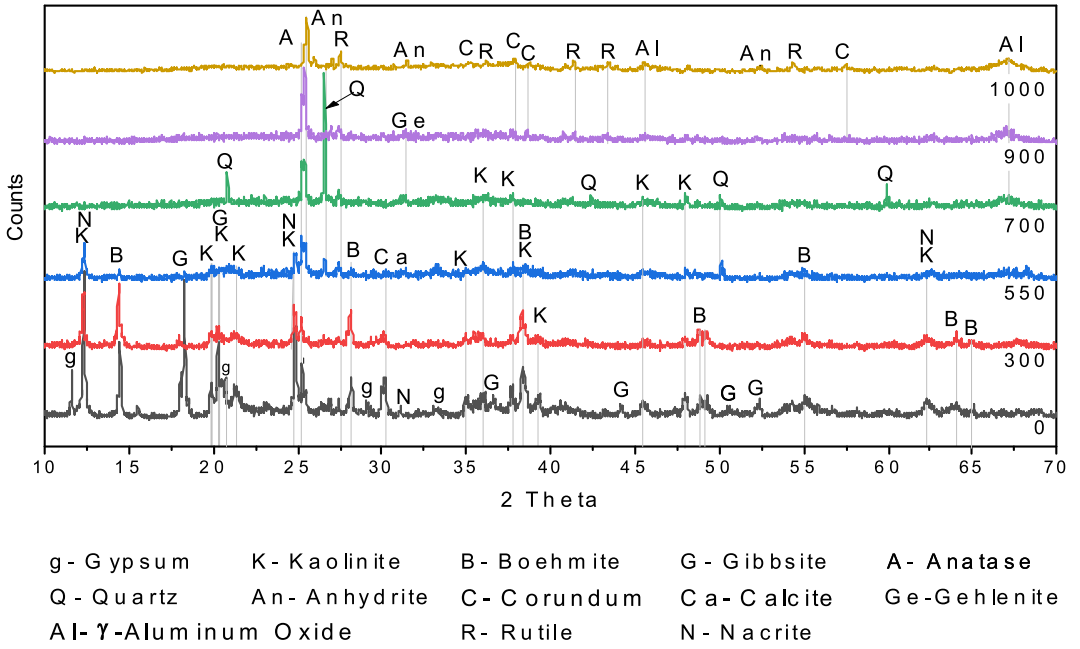

Fig. 2. XRD trace showing the crystalline phases the raw bauxite including gibbsite, kaolinite and boehmite with minor gypsum, rutile/anatase, nacrite and calcite.

Table 4
Mineral composition of the bauxite by XRD.

	Major phases (40-15%) Subsidiary (15-7%) Traces <7%		
Bauxite	Gibbsite - Al $(OH)_3$	Goethite $Fe_2O_3{\cdot}H_2O$ Gypsum - $CaSO_4{\cdot}2H_2O$	Quartz SiO_2
	Boehmite - ϒ- AlO(OH)	Rutile/anatase - TiO_2	
	Kaolinite - $Al_2Si_2O_5(OH)_4$/Nacrite	Calcite $CaCO_3$	

a result, nacrite has a lower stability and it is more reactive than kaolinite [29]. Cahyono and Damayanti [30] report significant nacrite in Indonesian bauxite. The authors state that nacrite is highly reactive in an alkaline environment, and that its presence increases the refining (Bayer process) costs due to both, the high dissolution of the nacrite's silica increasing the consumption of caustic soda, and its subsequent re-precipitation requiring desilication.

In the context of the present study, the high kaolinite content and the presence and highly-reactive, kaolinite-polymorph nacrite is likely an advantage, as these can enhance the reactivity of the bauxite in pozzolanic reactions.

Table 5
Mineral assemblages of the raw and thermally activated bauxites analysed with XRD, and phase changes on increasing activation temperature. C_4AF = tetracalcium aluminoferrite = $4CaO{\cdot}Al_2O_3{\cdot}Fe_2O_3$ (brownmillerite). C_3A = tricalcium aluminate.

Material	Phase composition by XRD major (40-15%) subsidiary (15-7%) traces <7%			Phase evolution
Bauxite	Gibbsite Al $(OH)_3$ Boehmite ϒ- AlO(OH) Kaolinite/Nacrite $Al_2Si_2O_5(OH)_4$	Gypsum $CaSO_4{\cdot}2H_2O$ Rutile/anatase TiO_2 Calcite Goethite $Fe_2O_3{\cdot}H_2O$	Quartz SiO_2	–
Bauxite 300 °C	Kaolinite ↓ Boehmite ↑	Calcite Nacrite↓	Magnetite Fe_2O_4 Quartz (SiO_2) Gypsum $CaSO_4{\cdot}2H_2O$	Gibbsite has disappeared transforming into boehmite. The amount of crystalline kaolinite has approximately halved with respect to the raw bauxite.
Bauxite 550 °C	Kaolinite ↓	Boehmite ↓	Quartz (SiO_2) Calcite Anhydrite Ca SO_4	The crystalline Al-containing phases lower but no new Al-containing phases appear. Hence, most of the Al is in amorphous form. Most of the crystalline boehmite and kaolinite have become amorphous ϒ- Al_2O_3 and metakaolin respectively.
Bauxite 700 °C	Quartz (SiO_2)	Kaolinite ↓ Rutile TiO_2 Anatase TiO_2	γ - Al_2O_3	Boehmite has disappeared. γ - Al_2O_3 peaks become evident.
Bauxite 900 °C	Corundum α Al_2O_3	Rutile TiO_2 Anhydrite Ca SO_4	γ - Al_2O_3 C_3A C_4AF Gehlenite $Ca_2Al_2SiO_7$ Anatase-TiO_2	Kaolinite has disappeared. Gehlenite appears. Possible traces of hydraulic C_3A /C_4A.
Bauxite 1000 °C	Corundum α Al_2O_3	Rutile/Anatase-TiO_2 Anhydrite Ca SO_4↓ Microcline	γ-Al_2O_3 C_3A C_4AF Gehlenite $Ca_2Al_2SiO_7$	Microcline appears. Possible traces of hydraulic C_3A /C_4A.

The mineralogical analysis results agree with Al-Dubasi [2]. According to the author, the Az Zabirah bauxite has a high alumina and silica content (average 56%, and 9% respectively), low iron content and a low organic matter content, and the alumina is boehmitic. The results also agree with Al Mutari et al., [3] that report gibbsite, boehmite, diaspore, kaolinite, hematite, quartz and calcite as the predominant minerals, with anatase (0.3–3.5%), zircon and rutile as minor minerals in the in the Az Zabirah bauxites. However, unlike other bauxites, no diaspore was clearly evidenced. Al Mutari et al., [3] state that diaspore can dissolve, and kaolinite recrystallize during the weathering of lateritic soils. The transformation of diaspore into kaolinite is probably the reason for the high kaolinite content and the lack of diaspore in the bauxite samples analysed.

4.3. Bauxite's phase changes with increasing sintering temperature

The mineralogy of the bauxite calcined at increasing temperature was analysed with XRD. Table 5 and Fig. 2 include the mineral assemblages obtained at each temperature, and the phase changes in the assemblage caused by increasing activation temperature.

Bauxite transformation at 300°C. The main events at 300 °C are as follows-Table 5:

- The gibbsite has disappeared transforming into boehmite agreeing with previous authors stating that, gibbsite dehydroxylation into boehmite occurs at ~300 °C (Alex et al., 2014) [9]. According to Zhang et al., 2019 [31], the transformation can be written simply as:

$$Al(OH)_3 \rightarrow AlOOH + H_2O$$

- The main kaolinite diffraction peaks have lost approximately half of their original relative intensities hence the amount of crystalline kaolinite has approximately halved with respect to the raw bauxite (by dehydroxilation according to the equation below).
- The lifting of the difractogram's baseline between approximately 19 and 22° (2Θ) (reaching a relative intensity of 15 counts) indicates the presence of an amorphous phase.

According to previous authors, the dehydroxilation of kaolinite to form amorphous metakaolinite begins after 400 °C and is completed at ~650 °C, though some additional mass loss can be observed up to 800 °C according to the equation: [32].

$$Al_2Si_2O_5(OH)_4 \rightarrow Al_2O_3 \bullet 2\ SiO_2 + 2H_2O$$

However, in this bauxite, the dehydroxylation begins at lower temperature (300 °C), at 550 °C most crystalline kaolinite has transformed, and at 700 °C it has totally disappeared. The lowering of the kaolinite dehydroxylation suggests an increase in reactivity, and it is probably due to the lower particle size and crystallinity of the bauxite. Crystallinity and particle size strongly influence the kaolinite transformation temperature, with small, poorly crystallized particles presenting lower dehydroxylation temperatures than high ordered samples with larger particles [33].

Bauxite transformation at 550°C. At 550 °C, most of the aluminium is in amorphous form. This is deducted as follows:

- The amount of crystalline, Al-bearing phases (kaolinite and boehmite) is very low: the relative intensities of their main reflections indicate than less than 30% of the original amount is present, ~70% of the boehmite has decomposed and ~37% of the kaolinite that was present at 300 °C has disappeared. Most of the crystalline boehmite and kaolinite have become amorphous ϒ- Al_2O_3 and metakaolin respectively. This agrees with Novák et al. [34] that state that boehmite is the thermodynamically stable phase up to approximately 300 °C and, if heated further in air, dehydration to y-alumina occurs.
- No new, crystalline, Al-bearing phases have formed.
- Therefore, most of the Al (at least 2/3rd s of the total content) is in amorphous form at 550 °C.
- The lifting of the difractogram's baseline (2Θ = 19–22°) reaching a relative intensity over 20 counts also indicates an increase in amorphous content.

Bauxite transformation at 700–1000°C. In the Saudi Arabian bauxite, γ-Al_2O_3 is present at 700, 900 and 1000 °C with blunt peaks located at 2Θ = 67.0° and 45.8°. **At 700°C,** γ - Al_2O_3 peaks have become evident however, most of the Al is still in amorphous form as, except for the ϒ- Al_2O_3 peaks, no other crystals of Al-bearing phases are present in the XRD pattern.

At 900 °C and 1000 °C, the amorphous alumina phases crystallize, becoming mainly the alpha polymorph corundum - α Al_2O_3-, and small amounts of gehlenite- $Ca_2Al_2SiO_7$. Microcline appears at the highest temperature and there are possible traces of aluminate and ferrite C_3A/C_4AF.

The mineral transformation of the alumina phases evidenced with XRD agrees with Sglavo et al. (2000) [35], Paglia (2004) [36] and others that studied the calcination path of transition aluminas, stating that boehmite transforms into γ-Al_2O_3 (present between 450 and 750 °C) and later into corundum according to the following sequence:

γ-Al_2O_3 → δ-Al_2O_3 (or gamma-prime-alumina (γ'-Al_2O_3) above 750 °C) → θ-Al_2O_3 → α-Al_2O_3 (corundum).

Gypsum -$CaSO_4 \cdot 2H_2O$- has become insignificant at 300 °C and has disappeared at 550 °C transforming into anhydrite -$CaSO_4$-. Gypsum enhances the pozzolanic reactivity of metakaolinite [37]. Therefore, the presence of anhydrite at 550 °C (temperature at which metakaolinite content is maximum) may enhance the bauxite's reactivity.

The phase change, caused by increasing activation temperature, in the bauxite's mineral assemblage analysed with XRD, places the highest reactivity at around 550 °C because, at this temperature, most of the aluminium is in amorphous form. However, even using advanced structural characterization techniques such as XRD, it is difficult to distinguish between amorphous and finely grained crystalline solids due to their similar interatomic distances. Amorphous materials have some short-range atomic order and, in very

small crystals, a large fraction of atoms are at or near the surface, distorting atomic positions and decreasing structural order [38]. Therefore, reactivity at temperatures other than 550 °C can be underestimated if based on the amorphous fraction only.

4.4. Results of thermal analyses by DSC and TGA

The mineral transformations resolved with XRD above, agree with the two endothermic peaks at ~300° and 520 °C determined with TGA/DSC. The bauxite shows a marked endothermic peak at 300 °C (Fig. 3). As evidenced with XRD, this peak is due to the decomposition of gibbsite and its partial transformation into boehmite, and to the transformation of approximately half of the kaolinite into metakaolin. This is followed by a smaller endothermic peak at 520 °C whereby the bauxite absorbs heat for the decomposition of crystalline boehmite (likely into amorphous ϒ- Al_2O_3) and the conversion of the remining crystalline kaolinite into metakaolin. The small endothermic peak at approximately 100 °C likely corresponds to the elimination of water molecules adsorbed to the external surfaces of the particles of the original aluminium hydroxides and kaolinite (Fig. 3).

The TGA analysis in Fig. 3 shows two main episodes of mass loss with rising temperature. The first weight loss of ~7% of the original mass at around 300 °C coincides with the endothermic peak of the decomposition of gibbsite and the conversion of kaolinite into metakaolin. Another significant weight loss coincides with the endothermic peak at 520 °C marking the decomposition of crystalline boehmite and the conversion of the last kaolinite into metakaolin.

4.5. Reactivity by the Chapelle test

The Chapelle test measures the amount of lime fixed per gram of bauxite. Lime combination is due to cation exchange (between the ions on the bauxite minerals surfaces and the lime's Ca^{2+}) and pozzolanic reaction, hence it is a good indicator of reactivity. The results (Table 6) indicate that the bauxite calcined at 550 °C combines the most lime, closely followed by the bauxite sintered at 700 °C. Therefore, the bauxites sintered at 500 and 700 °C have the greatest initial reactivity. At 800 °C, the amount of combined lime slightly lowers, however it is still significant. The difference in the amount of lime combined by the bauxite calcined at 800 and 900 °C is insignificant. In addition, the pozzolanic index of the bauxite is high, considerably superior to other pozzolanic or hydraulic materials previously studied [25and39-41] (Table 7). The values are comparable to those in the literature. Ferraz et al. [42] reached values of 920–1560 mg $Ca(OH)_2$/g for metakaolin, placing the minimum reactivity at 700 mg $Ca(OH)_2$/g metakaolin.

The high pozzolanic index for bauxite when compared with RM and FA is largely due to the mineralogy of the bauxite including major kaolinite, gibbsite and boehmite. The major components of the bauxite's red mud are hematite, cancrinite -$Na_6\ Ca_2[(CO_3)_2|Al_6Si_6O_{24}]\cdot 2H_2O$, gibbsite - Al $(OH)_3$ and sodalite $Na_4\ Si_3Al_3\ O_{12}Cl$ [25] which, although reactive, combine less lime that the bauxite's aluminium phases in the short term.

The FA used for comparison (SiO_2 = 53–65%; Al_2O_3 = 21–24%) contains significant amorphous material and some crystalline phases including quartz (SiO_2) and a small amount of mullite ($2Al_2O_3$. $2SiO_2$) [39]. As it can be evidenced from the Chapelle results, these combine less lime than the aluminium phases in the bauxite. As expected, the GGBS shows a poor lime combination, because the Chapelle test is not designed for latent hydraulic materials such as GGBS which would release lime on hydration, rather than combining it.

4.6. Reactivity by conductivity loss

This method follows the pozzolanic reaction indirectly by measuring the changes in the conductivity of saturated lime/bauxite solutions. The fixation of dissolved $Ca(OH)_2$ by the bauxite reduces the lime concentration in solution leading to a decrease in conductivity. The speed of consumption of portlandite (Fig. 4) was monitored over the first 170 h, hence it corresponds to the early rate of pozzolanic reaction. According to the results (Fig. 4), all the sintered bauxites combine substantial lime early, except for the bauxite calcined at 1000 °C, probably due to the presence of abundant crystalline corundum, and traces of hydraulic C_3A and C_4AF.

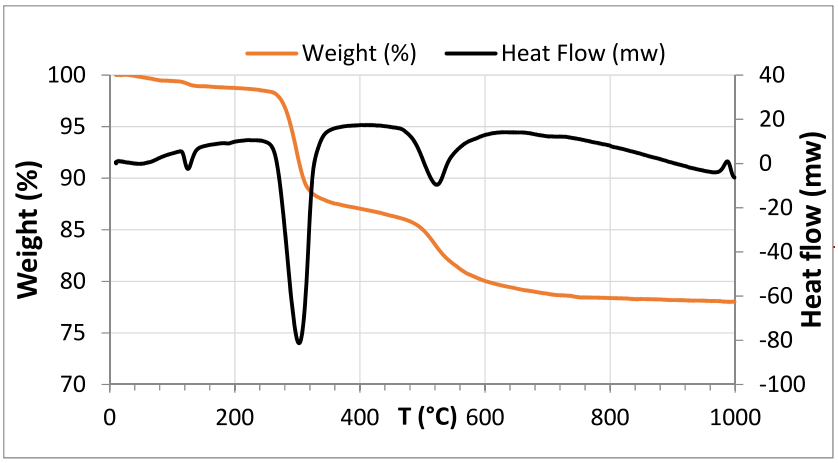

Fig. 3. Differential scanning calorimetry (DSC) and thermal gravimetric analysis (TGA) of the bauxite.

Table 6
Amount of lime fixed per gram of bauxite and pozzolanic index (I $Ca(OH)_2$ of both raw and calcined (300–1000 °C) bauxite specimens measured with the Chapelle test.

	Bauxite	Bauxite300	Bauxite550	Bauxite700	Bauxite800	Bauxite900	Bauxite1000
mg $Ca(OH)_2$/g	525	635	1034	996	819	808	425
mg CaO/g	397	481	783	755	620	612	322
I $Ca(OH)_2$	262	317	517	498	409	404	213

Table 7
Pozzolanic index –I $Ca(OH)_2$ – of the bauxite (B) compared with its red mud (RM) activated at temperatures ranging from 300 to 1000 °C; GGBS- ground granulated blast furnace slag-, FA-fly ash-, MK – metakaolin- and SCBA-sugar cane bagasse ash-. (*) Alelweet and Pavia 2020 [39]; (**) Alelweet and Pavia 2019 [40]; ($^{+}$) Berenguer et al., 2020 [41]. ($^{++}$) Alelweet et al., 2021 [25].

	B	B 300	B 550	B 700–800	B 900	B 1000	RM300-400 ++	RM750 ++	RM1000 ++	GGBS **	FA *	SCBA +	FA +	MK +
I $Ca(OH)_2$	262	317	517	498–409	404	213	203–229	127	140	104	286	293–337	382	1194

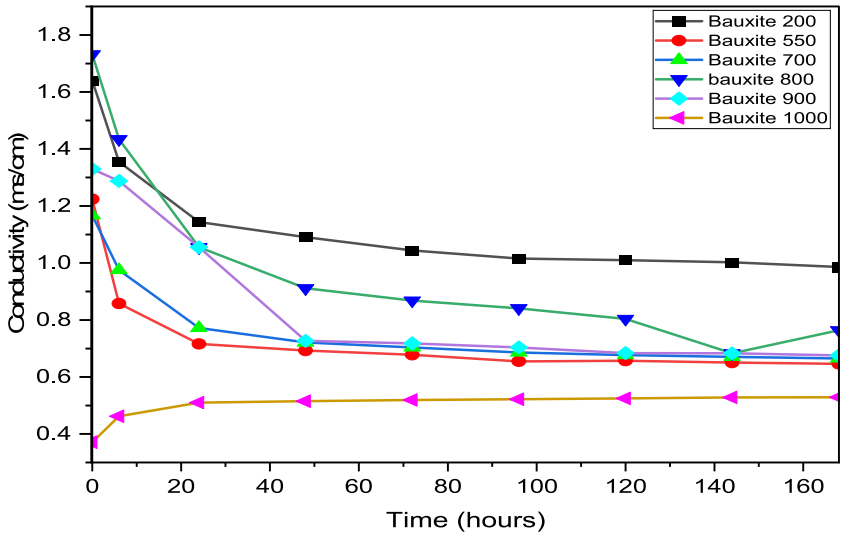

Fig. 4. Pozzolanic activity of the bauxite as change in conductivity of a saturated lime/bauxite solution (caused by lime consumption) over time or chemical activity index.

A slow fall in conductivity indicates a reduced chemical activity in the solutions, hence the bauxite is not combining lime and pozzolanic activity is low. On the contrary, the curves of the bauxites burned at 550, 700 and 800 °C show marked slopes in the first 6 h, evidencing significant activity. The conductivity loss of the bauxite sintered at 300 °C is significant, indicating that the bauxite calcined at lower temperature is also reactive. The curve of the bauxite burned at 900 °C is less steep, indicating lesser lime combination and hence less reactivity. The higher crystallinity and the incipient hydraulic phases recorded with XRD in the bauxite burned at 900 °C conform with this result.

The conductivity curves generally show that, within 48 h, most of the lime in solution has been consumed, and lime combination has either stopped or reduced significantly. This roughly agrees with McCarter and Tran [43] who established the reaction limit to 36 h

Table 8
Relationship between the water demand to produce an initial flow diameter of 170 ± 5 mm for a 1:1, bauxite: lime mix, setting times of the mixes, and specific surface area of the bauxite. (*) Scrivener and Capmas (1998) [1].

	T °C	W/b	SSA (m^2/g)	Initial Setting Time (h)	Final Setting Time (h)
Bauxite	300	0.61	81.81	5.6	6.1
	550	0.73	82.26	4.0	4.3
	700	0.73	82.53	0.8	1.3
	800	0.71	80.00	1.3	1.6
	900	0.65	67.00	5.1	5.5
	1000	0.62	40.38	5.5	6.6
CL90s	–	0.52	–	6.0	6.1
CEM I*	–	–	–	3 ± 1.20	4 ± 1.10
CAC*	–	–	–	3.55 ± 0.35	4.10 ± 0.35

for pozzolans such as RHA, GGBS, FA and MS. However, the bauxite burned at 200 °C reacts more slowly and activity ends after ~72 h. With the exception of the 1000 °C bauxite, the variation in conductivity over time is significant. According with this variation, the materials can be classified as having good pozzolanicity, as the variation in conductivity greater than 1.2 mS/cm [21].

4.7. Setting times and water demand

It is well known that water demand is largely determined by the specific surface area (SSA) of the particles. This is evidenced from the results -table 8- as the water demand is highest when the particles have greatest SSAs. As it can be seen from Table 8, sintering the bauxite up to 800 °C doesn't affect significantly neither the particle SSA nor the water demand of the paste. However, at higher temperature, both the SSA and water demand lower. This agrees with the XRD mineral assemblage showing that, at around 800 °C, the high SSA minerals such as kaolinite, boehmite and gibbsite have completely disappeared, and dense stable phases such as corundum have formed instead. The results -table 8- roughly agree with the mineral composition placing the maximum content of layered, high-SSA minerals (kaolinite/nacrite and boehmite) between 300 and 550 °C.

All the bauxites reduced the initial setting time of the hydrated lime, and they also shortened the final setting time (except for the 1000 °C bauxite). The bauxites sintered at 700 and 800 °C speed up the initial and final set of the hydrated lime significantly. The initial set of the 700 °C bauxite is ~7 times shorter than that of the lime (4.5 times shorter for the 800 °C bauxite). The final setting times also shorten significantly: the paste made with the bauxite sintered at 700 °C sets 4.6 times faster than the lime alone, 3.7 faster for the 800 °C bauxite paste. The bauxites sintered at 300 and 1000 °C reach their initial set faster than the hydrated lime, and their final set is either similar (300 °C) or slightly slower (1000 °C). According with EN 196–3 [17], the initial setting time shall be not less than 2 h, and the final setting time not more than 8 h. Therefore, all the final setting times comply with standard requirements. However, the initial set of the bauxites sintered at 700 and 800 °C is too quick.

Typically, it takes approximately 1 h for CEM I to achieve its final set. In contrast, all the bauxite pastes, except for 1000 °C paste, have achieved their final set within an hour. This agrees with previous research stating that pozzolans with highest Al_2O_3 content initially set the fastest [44] and that aluminates are responsible for the early set of a paste [45]. This was to be expected given the high aluminum content of the bauxite, and it is clearly evidenced in CACs which, even though they take similar time to initially set than PC, they reach their finial set much faster than PC due to their high aluminate content [1].

4.8. Reactivity by strength development and mechanical activity index

All the bauxites increased the 28-day compressive strength of the lime mix, and most of the bauxites surpassed the flexural strength of the hydrated lime (Table 9). The bauxites sintered at 800 and 900 °C produced the highest mechanical activity indices, followed by the bauxites sintered at 700 °C (37% MI reduction when compared to the 800 °C bauxite). The MI of the bauxite sintered at 800 and 900 °C is high. It compares well with highly-siliceous, pozzolanic materials such as rice husk ash and microsilica (Table 10), and it is lower than latent hydraulic materials such as GGBS and the eminently pozzolanic metakaolin.

As seen in the Chapelle test the bauxite has a higher pozzolanic index than its RM residue (Table 7), but their MIs are comparable (9–11 vs 7–8) – Table 10. This agrees with previous authors stating that compressive strength and hence the MI, is not only dependant on the amount of combined lime but also on the packing effect induced by the pozzolan and the microstructure of the hydration products formed [44].

4.9. Microstructure and reactivity by SEM/EDX

The microstructure of (1:1) pastes made with bauxite and hydrated lime (CL90s) are examined with SEM. The bauxites calcined at 550 and 700 °C were selected because, according to the XRD results, most of the silica in the raw bauxite (which is forming part of kaolinite - $Al_2Si_2O_5(OH)_4$/Nacrite) becomes amorphous in the 550–800 °C interval.

According to the XRF results, in the bauxite: lime system studied, the silica content is medium to low, ranging between 27 and 15%. Generally, the reaction of lime-pozzolan mixes produces the same compounds as those formed upon PC hydration, since the overall chemistry falls within the same field [46]. Therefore, in the alkaline conditions created by the lime, the amorphous silica and alumina phases dissolve and combine with the lime's Ca^{2+} to produce cementing hydrates: calcium silicate hydrates (C–S–H), calcium aluminate hydrates (C–A–H), and calcium alumino– silicate hydrates (C-A–S-H).

According to the SEM results, there are no measurable differences between the bauxite pastes at 550 and 700 °C. They both show relatively dense structures with abundant hydrates. However, rare unreacted alumina phases were observed in the 550 °C pastes

Table 9
Strength (28 d) and mechanical index of the bauxite at increasing temperature. SD−standard deviation.

Bauxite	Flexural strength (MPa)	*SD*	Compressive strength (MPa)	*SD*	Mechanical index	
						W/b
300 °C	0.26	*0.01*	0.55	*0.05*	1.80	0.85
550 °C	0.19	*0.02*	0.45	*0.03*	1.47	1.00
700 °C	0.33	*0.04*	0.93	*0.05*	3.05	1.05
800 °C	1.31	*0.06*	3.51	*0.08*	11.52	0.83
900 °C	1.17	*0.14*	2.83	*0.26*	9.29	0.77
1000 °C	0.47	*0.04*	0.64	*0.03*	2.10	0.73
lime	0.17	*0.05*	0.30	*0.05*	–	1.07

Table 10
MI of the bauxite compared with the MI of the bauxite's red mud -RM- (sintered at 300–750 °C) and other pozzolanic/cementing materials. * Alelweet et al., 2021 [25]. + Walker and Pavia 2011 [44]. RHA- Rice husk ash; MS- microsilica; MK-metakaolin; BD-brick dust.

	Bauxite300	Bauxite700	Bauxite800/900	RM300*	RM400&750*	FA^{+}	GGBS^{+}	RHA^{+}	MS^{+}	MK^{+}	BD^{+}
MI	1.8	3	11.5/9.29	8	7	3.5	29	12	12	38	2–3

(Fig. 5). The pozzolanic pastes show abundant pozzolanic hydrates and occasionally relics of pseudo-hexagonal plates and rhombic plates of very low crystallinity which are probably the remains of untransformed boehmite and metakaolinite (Fig. 6). Metakaolinite is usually almost amorphous. However, the particles retain the pseudo-hexagonal morphology, and structural order persists within individual layers but not between them [33]. Ghosts of hexagonal and rhombic habits covered by abundant pozzolanic hydrates of low crystallinity are also present (Figs. 7 and 8). Figs. 9 and 10 include the elemental analyses of the phases and cements above.

The microstructure of the bauxite: lime pastes investigated show similarities with those of thermally-treated, clay sediments, activated in stronger alkaline media (such as NaOH solutions) to produce geopolymeric materials [47,48].

5. Discussion

The results (Table 11) show that the bauxite is remarkably pozzolanic, and that traces of hydraulic phases are only evidenced when the bauxite is sintered over 900 °C.

The bauxite mainly consists of gibbsite, kaolinite and boehmite. The amount of gibbsite is close to the amount of kaolinite, and the amount of boehmite is at least 50% lower. The layered atomic structures of gibbsite, boehmite and kaolinite, with high specific surfaces and active surface hydroxyls that enhance adsorption, and hence nucleation, precipitation and dissolution, are the main drivers of the pozzolanic activity. The high reactivity of the bauxite is assisted by the great SSA of its particle constituents (superior to CEM II and other pozzolans), and by their high fineness produced with milling.

The early dehydroxilation of the kaolinite in the bauxite subject to study (beginning at 300 °C and completed at 700 °C), indicates high reactivity. The high kaolinite content of the bauxite, and the presence and the high-reactivity, kaolinite-polymorph, nacrite further enhanced the pozzolanic reactivity. According to Heller-Kallai [37], sulphates improve the pozzolanic reactivity of metakaolinite. Therefore, the presence of sulphates (gypsum turning into anhydrite at 550 °C) has probably improved the pozzolanic activity of the bauxite by increasing the activity of metakaolinite at ~700 °C (temperature at which metakaolinite content is maximum).

Some of the results indicate initial activity (SSA, Chapelle test, conductivity variation and setting times) while others indicate later activity (28-day strength and mechanical index). A high SSA makes lime combination easier in the earlier stages of the pozzolanic reaction, whereas at longer ages, the pozzolanic reaction is mainly controlled by the active silica and alumina content [46]. The Chapelle, conductivity and setting times tests measure the ability to combine lime in the first hours hence the initial reactivity. In this research, the SSA, Chapelle and conductivity results agree. The Chapelle tests evidenced that the bauxite calcined at 550 °C combines the most lime, hence showing the greatest initial activity, closely followed by the bauxite sintered at 700 °C, and the bauxites sintered at 550 °C and 700 °C showed the greatest specific surface areas. The conductivity results agree, as the conductivity curves of the 550, 700 and 800 °C bauxites show marked slopes in the first 6 h evidencing high activity.

All the bauxites reduced the initial setting time of the hydrated lime, and they also shortened the final setting time of the lime (except for the 1000 °C bauxite). The 550 °C bauxite takes slightly longer to initially set when compared to the bauxites calcined at 800–900 °C however, it reached its final set within 20 min (agreeing with the quick lime binding of the sample shown by the Chapelle and conductivity tests) and its setting times comply with current standard requirements.

The bauxites sintered at 800 and 900 °C produced the highest strengths and mechanical activity indices, followed by the 700 °C bauxite (with a 37% reduction). This agrees with the XRD results whereby the bauxite sintered at 700–800 °C, contains the highest amorphous/active alumina content because the boehmite has totally disappeared, transformed into amorphous transition aluminas, and the kaolinite has completely turned into reactive metakaolin (kaolinite disappeared before 900 °C). Therefore, the results agree with Massaza [45] who states that strength and mechanical index indicate late pozzolanic activity where the pozzolanic reaction is mainly controlled by the active silica and alumina content.

The thermal analyses concur with the XRD results, indicating two main endothermic events at 300 °C (marking gibbsite decomposition into boehmite, and transformation of approximately half of the kaolinite into metakaolin) and at 520 °C (decomposition of boehmite and transformation of the remining kaolinite into metakaolin).

At 900 °C corundum is the main phase, and traces of hydraulic phases and gehlenite begin to appear. The sudden drop in SSA and the transformation of the alumina phases into stable, unreactive crystalline corundum lower pozzolanic activity and reduce strength.

6. Conclusion

The environmental impact of PC production (even with partial clinker substitution) is enormous when compared with the impact of bauxite mining. (CEM II releases 620–700 kg CO_2e/t *vs* 3–5 kg CO_2e/t for bauxite mining).

Gibbsite, boehmite and kaolinite are the main phases in the Saudi Arabian bauxite. The layered atomic structures of gibbsite and boehmite are comparable to the structure of clay mineral kaolinite, featuring high specific surfaces and active surface hydroxyls that enhance adsorption, and hence nucleation, precipitation and dissolution, which makes them highly reactive.

All the tests evidenced a high pozzolanic activity for the bauxite. The pozzolanic index (Chapelle method) is high, superior to other

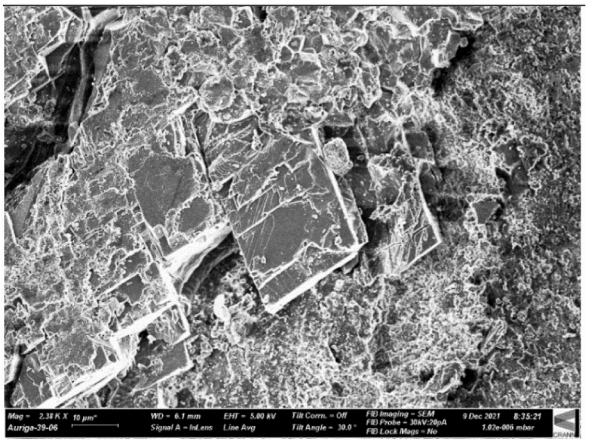

Fig. 5. Microstructure of the (1:1) paste made with 550 °C bauxite and hydrated lime (CL90s) showing un-reacted boehmite with a rhombic habit covered with hydrates.

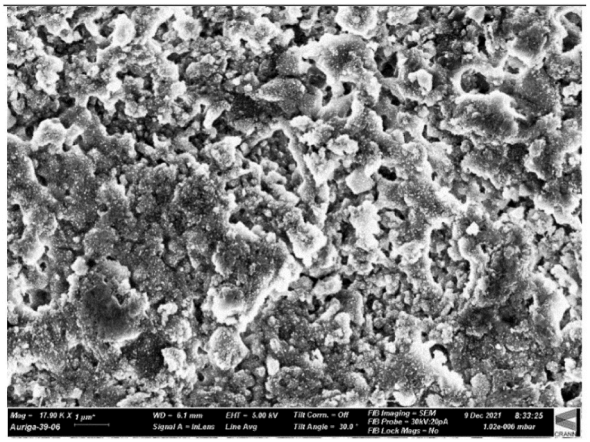

Fig. 6. Abundant pozzolanic precipitates and relics of pseudo-hexagonal plates of metakaolinite and rhombic plates (remains of boehmite not yet transformed), in the paste made with lime (CL90s) and bauxite calcined at 550 °C.

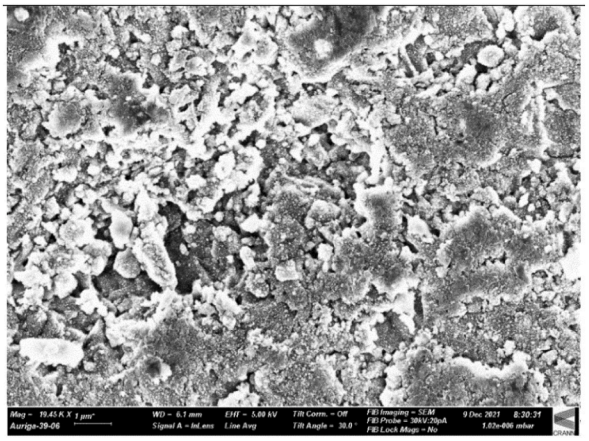

Fig. 7. Abundant pozzolanic precipitates leading to a lower porosity in the (1:1) paste made with lime (CL90s) and bauxite calcined at 700 °C.

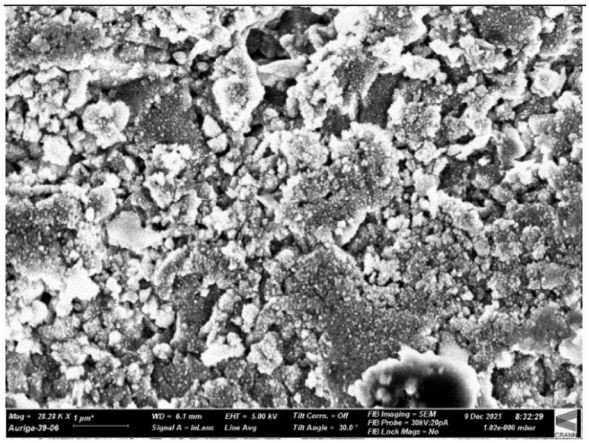

Fig. 8. Ghosts of hexagonal and rhombic habits covered with abundant pozzolanic hydrates of low crystallinity-also seen in Fig. 7.

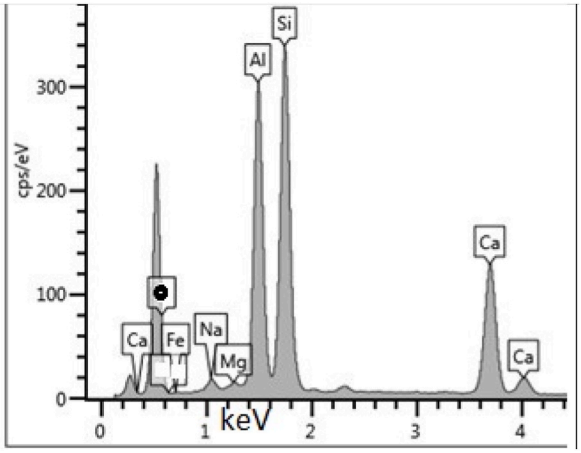

Fig. 9. Elemental composition analysis of the binder in Fig. 7 by EDS.

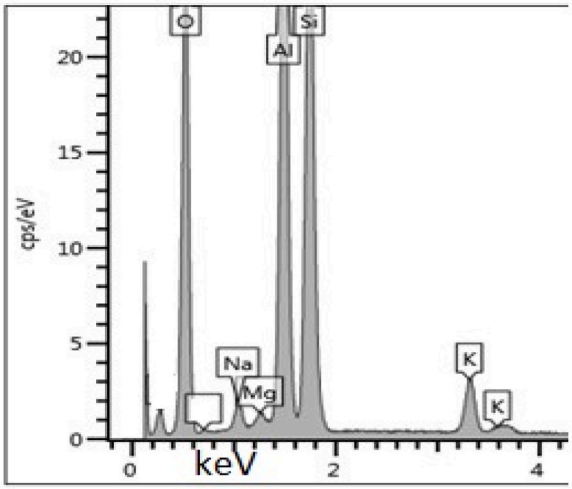

Fig. 10. Elemental composition analysis of hexagonal plates (Fig. 6 and 8) by EDS.

Table 11
Summary of main results.

Bauxite	SSA (m^2/g)	Chapelle test Ca $(OH)_2$/g	Setting times (min)		CS (MPa)	MI	Phase evolution (XRD)
			Initial	Final			
300 °C	81.81	635	340	370	0.55	1.80	Gibbsite disappeared transforming into boehmite. 50% kaolinite disappeared becoming metakaolinite.
550 °C	82.26	1034	240	260	0.45	1.47	Most of the Al phases are amorphous. Most of the crystalline boehmite and kaolinite have become amorphous ϒ- Al_2O_3 and metakaolin.
700 °C	82.53	996	50	80	0.93	3.05	Boehmite has disappeared (completely transformed into amorphous
800 °C	80.00	819	80	100	3.51	11.52	transition aluminas) γ - Al_2O_3 peaks become evident.
900 °C	67.00	808	310	330	2.83	9.29	Kaolinite has disappeared. γ - Al_2O_3 is present but some alumina phases have become corundum. Possible traces of C_3A, C_4AF and gehlenite
1000 °C	40.38	425	330	400	0.64	2.10	Corundum increases. Microcline appears. Possible traces of C_3A, C_4AF and gehlenite.

pozzolanic materials previously studied, and the mechanical index compares well with other pozzolanic and cementing materials. All the bauxites increased the 28-day compressive strength of the standard, hydrated-lime mix.

The high specific surface area of the bauxite particles, confirmed with laser diffraction, is superior to CEM II and other pozzolanic and cementing materials such as FA and GGBS. Heating, even at low temperature, significantly increases the SSA of the bauxite particles (at 300 °C the SSA rises by over 60%).

The high kaolinite content (likely secondary from diaspore dissolution), and the presence of highly-reactive, kaolinite-polymorph nacrite, enhance the reactivity of the Saudi bauxite in pozzolanic reactions. The presence of sulphates (minor-traces) also contributes to the initial activity.

The kaolinite in the Saudi bauxite begins to dehydroxylate at 300 °C, significantly earlier than reported by previous authors, evidencing an increased reactivity which is probably assisted by the presence of nacrite and sulphates, and the ultrafine particle fraction produced by milling.

The results of the SSA, Chapelle test, conductivity variation and setting time tests indicate the initial pozzolanic activity of the bauxite, while the results of the 28-day strength and the mechanical index indicate the amount of late pozzolanic activity.

The methods that determine the initial pozzolanic activity rate the 550 °C bauxite as the most active, while the mechanical methods rate the 700–800 °C bauxites as the most reactive. This is because the 550 °C bauxite has one of the highest SSAs that makes lime combination easier in the earlier stages of the pozzolanic reaction, hence it combines the most lime in the Chapelle and conductivity tests. However, when sintered at 700–800 °C, the bauxite contains the highest amorphous/active alumina content (which control the late pozzolanic activity), because at 700–800 °C the boehmite has totally disappeared, transformed into amorphous transition aluminas, and the kaolinite has completely turned into reactive metakaolin.

Author statement

Omar Alelweet Testing and analyses. Background research, Sara Pavia Supervision. Writing- Reviewing and Editing.

Declaration of competing interest

The authors declare that they have no known competing financial interests or personal relationships that could have influenced the work reported in this paper.

Acknowledgements

The authors thank Baba Ahmed Mohamed Sidiya, from Kaolin Processing and Management, and Abdul Malik Shaheen, Ma'adem Industries, for providing valuable information of the mining and the processing and refining processes of the bauxite, and Ali Mohammed Al Sarar, Yousef Al Hindi, Yusef Mesfer Al Harbi and Bander Abdullah Al-Harbi for assisting with the sampling. The authors also thank the Government of Saudi Arabia, Technical & Vocational Training Corporation and the Saudi Arabian Cultural Bureau for their support and for financing the project. We thank our colleagues in the Civil Engineering laboratories in particular, M. O'Shea, M. Grimes, our Chief Technician D. McAuley and M. Gilligan for their assistance with testing. The authors thank Dr R. Goodhue of ICRAG/Geochemistry TCD, Dr J. Canavan, Geography Department, TCD, D. Daly of AMBER, the SFI Research Centre for Advanced Materials and BioEngineering Research and CRANN Institute, TCD, and Dr A. Rafferty, AMBER,CRANN Institute, for their assistance with the analyses.

References

[1] K.L. Scrivener, A. Capmas, Calcium aluminate cements. Lea's chemistry of cement and concrete, in: P.C. Hewlett (Ed.), Lea's Chemistry of Cement and Concrete, fourth ed., Elsevier, 1998.
[2] A. Al-Dubaisi, Development of bauxite & alumina resources in the kingdom of Saudi Arabia, in: S.J. Lindsay (Ed.), Light Metals 2011, Springer, Cham, 2011, https://doi.org/10.1007/978-3-319-48160-9_4.
[3] Al-Mutairi, M.A. Galmed, K.S. Aldamegh, Petrogenesis of the Az Zabirah south zone bauxite ore deposits, central northern Saudi Arabia A N, Arabian J. Geosci. 8 (2015) 2327–2339, https://doi.org/10.1007/s12517-014-1347-5.
[4] J. Rosenqvist, Surface Chemistry of Al and Si (Hydr)oxides, with Emphasis on Nano-Sized Gibbsite (α-Al(OH)3) Department of Chemistry, in: Printed by Solfjädern Offset AB Umeå, Inorganic Chemistry Umeå University, Umeå, Sweden, 2002, ISBN 91-7305-245-0.
[5] K. Hadjiivanov, Identification and characterization of surface hydroxyl groups by infrared spectroscopy, in: Friederike C. Jentoft (Ed.), Advances in Catalysis vol. 57, Academic Press, 2014, pp. 99–318, https://doi.org/10.1016/B978-0-12-800127-1.00002-3.
[6] M. Lagauche, K. Larmier, E. Jolimaitre, K. Barthelet, C. Chizallet, L. Favergeon, M. Pijolat, Thermodynamic characterization of the hydroxyl group on the γ-alumina surface by the energy distribution function, J. Phys. Chem. 121 (31) (2017) 16770–16782, https://doi.org/10.1021/acs.jpcc.7b02498.
[7] S. Brühne, S. Gottlieb, W. Assmus, E. Alig, M.U. Schmidt, Atomic structure analysis of nanocrystalline boehmite AlO(OH) cryst, Growth Des 8 (2) (2008) 489–493, https://doi.org/10.1021/cg0704044.
[8] X. Zhang, P.L. Huestis, C.I. Pearce, J Zhi Hu, K. Page, L.M. Anovitz, A.B. Aleksandrov, M.P. Prange, S. Kerisit, M.E. Bowden, W. Cui, Z. Wang, N.R. Jaegers, T. R. Graham, M. Dembowski, H.W. Wang, J. Liu, A.T. N'Diaye, M. Bleuel, D.F.R. Mildner, T.M. Orlando, G.A. Kimmel, JA La Verne, S.B. Clark, K.M. Rosso, Boehmite and gibbsite nanoplates for the synthesis of advanced alumina products, ACS Appl. Nano Mater. 1 (12) (2018) 7115–7128DOI, https://doi.org/10.1021/acsanm.8b01969, 2018.
[9] T.C. Alex, Rakesh Kumar, S.K. Roy, S.P. Mehrotra, Mechanically induced reactivity of gibbsite: Part 1, Planetary milling, Powder Technology 264 (2014) 105–113, https://doi.org/10.1016/j.powtec.2014.05.028, 2014.
[10] K. Georgitzikis, L. Mancini, E. d'Elia, B. Vidal-Legaz, Sustainability Aspects of Bauxite and Aluminium Joint Research Centre (JRC), Technical Report, 2021.
[11] T. Norgate, N. Haque, Energy and greenhouse gas impacts of mining and mineral processing operations, J. Clean. Prod. 18 (2010) 266–274, https://doi.org/10.1016/j.jclepro.2009.09.020.
[12] P. Sheik Mujabar, S. Dajkumar, Mapping of bauxite mineral deposits in the northern region of Saudi Arabia by using Advanced Spaceborne Thermal Emission and Reflection Radiometer satellite data, Geo Spatial Inf. Sci. 22 (1) (2019) 35–44, https://doi.org/10.1080/10095020.2018.1530857.
[13] B.M.A. Sidiya, Environmental Carbon Emissions of Bauxite Mining in the Mines of Az Zhabira, Kaolin Processing and Management. Ma'aden Industries, 2021 unpublished report.
[14] B.L. Damineli, F.M. Kemeid, P.S. Aguiar, V.M. John, Measuring the eco-efficiency of cement use, Cement Concr. Compos. 32 (8) (2010) 555–562, https://doi.org/10.1016/j.cemconcomp.2010.07.009.
[15] R.I.C. Juarez, S. Finnegan, The environmental impact of cement production in Europe: a holistic review of existing EPDs, Cleaner Environmental Systems 3 (2021) 100053, https://doi.org/10.1016/j.cesys.2021.100053.
[16] D. García-Gusano, I. Herrera, D. Garraín, Y. Lechon, H. Cabal, Life cycle assessment of the Spanish cement industry: implementation of environmentally friendly solutions, Clean Technol. Environ. Policy 17 (2015) 59–73, https://doi.org/10.1007/s10098-014-0757-0.
[17] EN 196-3:2016 Determination of Setting Times and Soundness.
[18] EN 196-1:2016 Determination of the Compressive and Flexural Strength of Cement Mortar.
[19] EN 450-1:2012 Fly Ash for Concrete.
[20] R. Lima Figueiredo, S. Pavia, A study of the parameters that determine the reactivity of sugarcane bagasse ashes (SCBA) for use as a binder in construction, SN Appl. Sci. 2 (1515) (2020).
[21] M.P. De Luxan, F. Madruga, J. Saavedra, Rapid evaluation of pozzolanic activity of natural products by conductivity measurement, Cement Concr. Res. 19 (1989) 63–68, https://doi.org/10.1016/0008-8846(89)90066-5.
[22] J. Paya, M.V. Borrachero, J. Monzo, E. Peris-Mora, F. Amahjour, Enhanced conductivity measurement techniques for evaluation of fly ash pozzolanic activity, Cement Concr. Res. 31 (1) (2001) 41–49, 2001.
[23] G.P. Gava, L.R. Prude, Pozzolanic activity tests as a measure of pozzolans performance, Part 1', Magazine of Concrete Research 59 (10) (2007) 729–734, https://doi.org/10.1680/macr.2007.59.10.729.
[24] NBR 15895, Método Chapelle Materiais pozolânico - determinagáo do teor modificado de hidróxido de cálcio fixado, in: Associação Brasileira de Normas Técnicas, 2010, p. 209.
[25] O. Alelweet, S. Pavia, Z. Lei, Pozzolanic and cementing activity of raw and pyro-processed Saudi arabian red mud (RM) waste, Recent Progress in Material 3 (4) (2021) 26, https://doi.org/10.21926/rpm.2104047.
[26] A.C. Vieira Coelho, H. Souza Santos, P.K. Kiyohara, P. Souza Santos, Surface area and crystal morphology of alumina powders by thermal activation of a gibbsite precursor prepared by a new procedure, CBECIMAT (2002) 1534–1538.
[27] L.J. Poppe, V.F. Paskevich, J.C. Hathaway, D.S. Blackwood, A laboratory manual for X-ray powder diffraction. Kaolinite group minerals. U. S. Geological survey open-file report 01-041 coastal and marine geology program, Woods Hole Field Center, MA 02543-1598 508 (2001) 548–8700.
[28] J. Kloprogge, Introduction, in: Spectroscopic Methods in the Study of Kaolin Minerals and Their Modifications, Springer Mineralogy. Springer, Cham, 2019, https://doi.org/10.1007/978-3-030-02373-7_1.
[29] M.F. Brigatti, E. Galan, B.K.G. Theng, in: F. Bergaya, B.K.G. Theng, G. Lagaly (Eds.), Structures and Mineralogy of Clay Minerals. Handbook of Clay Science, Developments in Clay Science, vol. 1, Elsevier Ltd, 2006.
[30] H.S.S. Cahyono, R. Damayanti, Upgrading of Tayan's crude bauxite using rotary drum scrubber, Indonesian Mining Journal 17 (No. 1) (2014) 40–52.
[31] X. Zhang, W. Cui, J Zhi Hu, H.W. Wang, M.P. Prange, C. Wan, N.R. Jaegers, M. Zong, H. Zhang, C.I. Pearce, P. Li, Z. Wang, S.B. Clark, K.M. Rosso, Transformation of gibbsite to boehmite in caustic aqueous solution at hydrothermal conditions, Cryst. Growth Des. 19 (10) (2019) 5557–5567, https://doi.org/10.1021/acs.cgd.9b00468.
[32] Ferreira da Costa Gardolinski, Interlayer Grafting and Delamination of Kaolinite, Doctoral Thesis. Univ of Kiel Germany, 2005.
[33] G.W. Brindley, J.P. Lemaître, in: A.C.D. Newman (Ed.), Thermal, Oxidation and Reduction Reactions of Clay Minerals in Chemistry of Clays and Clay Minerals, 1987, pp. 319–364.
[34] C. Novák, G. Pokol, V. Izvekov, Studies on the reactions of aluminium oxides and hydroxides, J. Therm. Anal. 36 (1990) 1895–1909, https://doi.org/10.1007/BF01913436, 1990.
[35] V.M. Sglavo, R. Campostrini, S. Maurina, G. Carturan, M. Monagheddu, G. Budroni, G. Cocco, Bauxite 'red mud' in the ceramic industry. Part 1: thermal behavior, J. Eur. Ceram. Soc. 20 (2000) 235–244.
[36] G. Paglia, C.E. Buckley, A.L. Rohl, Boehmite derived γ-alumina system. 1. Structural evolution with temperature, with the identification and structural determination of a new transition phase, γ-alumina, Chem. Mater. 16 (2) (2004) 220–236.
[37] L. Heller-Kallai, Thermally modified clay minerals. Handbook of clay science, in: F. Bergaya, B.K.G. Theng, G. Lagaly (Eds.), Developments in Clay Science, Elsevier, 2006. 10.1016/S1572-4352(05)01009-3.
[38] A. Varshneya, Fundamentals of Inorganic Glasses, Academic Press, Boston, 1994.
[39] O. Alelweet, S. Pavia, Potential of a low-calcium fly ash (FA) for the production of alkali-activated materials, in: Ruane, Vesna Jaksic (Eds.), Proc. Of the Civil Engineering Research in Ireland (CERI) Conference, Cork, August 2020, Civil Engineering Research Association of Ireland, 2020, pp. 162–168.
[40] O. Alelweet, S. Pavia, An evaluation of the feasibility of several industrial wastes and natural materials, as precursors, for the production of alkali activated materials, Int. J. Civ. Environ. Eng. 13 (12) (2019) 741–748, 2019.

[41] R. Berenguer, N. Lima, A.C. Valdés, M.H.F. Medeiros, N.B.D. Lima, J.M.P.Q. Delgado, F. Silva, A.N. Azevedo, A.C. Guimarães, B. Rangel, Durability of concrete structures with sugar cane bagasse ash, in: Advances in Materials Science and Engineering, vol. 2020, 2020, https://doi.org/10.1155/2020/6907834.
[42] E. Ferraz, S. Andrejkovičová, W. Hajjaji, A.L. Velosa, A.S. Silva, F. Rocha, Pozzolanic activity of metakaolins by the French standard of the modified Chapelle test: a direct methodology, Acta Geodyn. Geomater. 12 (No. 3) (2015) 289–298, https://doi.org/10.13168/AGG.2015.0026, 179, 2015.
[43] W.J. McCarter, D. Tran, Monitoring pozzolanic activity by direct activation with calcium hydroxide, Construct. Build. Mater. (1996) 179–184, https://doi.org/10.1016/0950-0618(95)00089-5.
[44] R. Walker, S. Pavía, Physical properties and reactivity of pozzolans, and their influence on the properties of lime-pozzolan pastes, Materials and Structures/Materiaux et Constructions 44 (6) (2011) 1139–1150, https://doi.org/10.1617/s11527-010-9689-2.
[45] F.W. Taylor, Cement Chemistry, Thomas Telford Publ, London, 1997.
[46] F. Massazza, Pozzolana and pozzolanic cements, in: P.C. Hewlett (Ed.), Lea's Chemistry of Cement and Concrete, fourth ed., Elsevier, UK, 1998, pp. 471–602.
[47] C. Ferone, B. Liguori, I. Capasso, F. Colangelo, R. Cioffi, E. Cappelletto, R. Di Maggio, Thermally treated clay sediments as geopolymer source material, Appl. Clay Sci. 107 (2015) 195–204, https://doi.org/10.1016/j.clay.2015.01.027.
[48] V. Medri, S. Fabbri, J. Dedecek, Z. Sobalik, Z. Tvaruzkova, A. Vaccari, Role of the morphology and the dehydroxylation of metakaolins on geopolymerization, Appl. Clay Sci. 50 (4) (2010) 538–545, https://doi.org/10.1016/j.clay.2010.10.010.